Elastic and inelastic scattering of 50-MeV pions from ^{28}Si and ^{30}Si

U. Wienands,* N. Hessey,† B. M. Barnett,‡ F. M. Rozon, H. W. Roser,§
A. Altman,** and R. R. Johnson
University of British Columbia, Vancouver, British Columbia, Canada V6T 2A3

D. R. Gill and G. R. Smith
TRIUMF, Vancouver, British Columbia, Canada V6T 2A3

C. A. Wiedner
Max Planck Institut für Kernphysik, D-6900 Heidelberg, Federal Republic of Germany

D. M. Manley††
Lawrence Livermore National Laboratory, University of California, Livermore, California 94550

B. L. Berman
Lawrence Livermore National Laboratory, University of California, Livermore, California 94550
and Department of Physics, The George Washington University, Washington, D.C. 20052

H. J. Crawford
University of California Space Sciences Laboratory, Berkeley, California 94720

N. Grion
Instituto Nazionale di Fisica Nucleare, I-34127 Trieste, Italy
(Received 19 September 1986)

Angular distributions of the differential cross section for elastic and inelastic scattering of 50-MeV π^+ and π^- on ^{28}Si and ^{30}Si have been measured to a relative accuracy of 5–10%. We fitted the cross section of elastic π^+ and π^- scattering from ^{28}Si simultaneously with an optical model using a second-order potential of the Michigan State University form. Our best-fit parameters differ from those given previously. The ratio of the neutron and proton transition-matrix elements for the first $J^\pi=2^+$ state in ^{28}Si is found from the inelastic cross section to be 1.13 ± 0.09. For ^{30}Si, the ratio is found to be 0.93 ± 0.09, which differs significantly from the value derived from lifetime measurements on mirror nuclei.

I. INTRODUCTION

In recent years pion scattering as a means of probing nuclear structure has been a topic of considerable interest. The two different isospin states of the charged pion make it a unique probe for separating isoscalar and isovector effects. Consequently, a number of pion-scattering experiments at resonance energy have been initiated that attempt to separate proton and neutron contributions to nuclear-matter distributions and transition-matrix elements (e.g., Refs. 1–3). For pions at kinetic energies near 160 MeV the pion-nucleon interaction is dominated by the P_{33} partial wave ($l=1$, $J=\frac{3}{2}$, $T=\frac{3}{2}$); therefore, the isospin vector-coupling coefficients give, for the ratio of scattering amplitudes for π^+p/π^-p and π^-n/π^+n, a value of 3, because (π^+p) and (π^-n) exist in a pure $T=\frac{3}{2}$ state, while (π^-p) and (π^+n) exist in a mixture of $T=\frac{3}{2}$ and $T=\frac{1}{2}$ states.

For lower pion energies however, the dominant partial waves are S_{11}, S_{31}, and P_{33}, which are comparable in magnitude but different in phase. Therefore, interference can occur; in fact, this gives a much higher, angle-dependent ratio, which reaches 20:1 for the scattering amplitudes of 50-MeV pions at backward angles, where the π^+ effectively scatter only from protons and the π^- only from neutrons.[4] This selectivity, in conjunction with the inherent symmetry of the π^+/π^- ratio experiments, makes low-energy pion scattering a valuable tool for investigating the isovector components of the nuclear structure. The sensitivity of various probes to protons and neutrons has been discussed extensively by Madsen and collaborators.[5–9]

Previous experiments measuring the ratio $d\sigma(\pi^+)/d\sigma(\pi^-)$ for scattering of low-energy pions to excited states have confirmed that similar selectivity also exists for nuclei. The ratios of the proton and neutron matrix elements obtained in these experiments generally are consistent with those obtained with other hadronic probes, such as medium-energy protons, but some inconsistencies between the values determined by different probes do exist.[4,7] These inconsistencies may indicate the necessity of Coulomb corrections, whose magnitude, however, is only poorly established.

Data from pion-scattering experiments are often analyzed by means of an optical model for elastic scatter-

ing. The same optical potential is then used in the distorted-wave impulse approximation (DWIA) calculation for inelastic scattering. For scattering at resonance energies, a first-order Kisslinger potential[10] with parameters derived from πN phase shifts describes the general features of the angular distribution quite well, despite the fact that such a potential does not contain terms which account for true pion absorption. Difficulties exist for higher transverse momenta. At low energies, a potential motivated by the second-order expansion of the multiple-scattering series, which includes true absorption and the Lorentz-Lorenz-Ericson-Ericson (LLEE) term describing short-range correlations, was obtained by Stricker, McManus, and Carr at Michigan State University (MSU) to describe the angular distributions for a range of nuclei.[11–13] The parameters of this potential were determined by a fit to the π^+ elastic cross sections and pionic-atom data which were available at that time.

In the present work the results of elastic and inelastic scattering of positive and negative pions from ^{28}Si and ^{30}Si are reported. The purpose of the experiment was two-fold. First, by providing the elastic cross sections for both π^+ and π^-, the existing data base for pion-nucleus scattering (especially for π^- scattering) is enlarged, which is necessary to determine the parameters of the optical potential used in the DWIA calculations. Secondly, and more important, the inelastic scattering to the first excited $J^\pi=2^+$ state allows one to measure the value of the ratio of the transition-matrix elements M_n/M_p to this state for the nuclei investigated. These values can be compared to those obtained with other probes, and differences can provide us with information regarding the reaction mechanisms involved.

II. EXPERIMENTAL TECHNIQUE

A. Apparatus

The experiment was carried out at the $M13$ low-energy pion channel at TRIUMF using the QQD spectrometer to detect the scattered pions. Both devices have been described in detail elsewhere;[14,15] thus only an overview of the relevant features is given here. Figure 1 shows the experimental setup.

The channel delivers a flux of about 2×10^6 $\pi^+/(s\times10^{-2}\Delta p/p)$ and 4×10^5 $\pi^-/(s\times10^{-2}\Delta p/p)$ at 100 μA proton current and 50 MeV pion energy to an achromatic focus with a spot size of 15×10 mm^2 full width at half maximum (FWHM). Usually, collimators at the intermediate chromatic foci $F1$ and $F2$ of the channel (see Fig. 1) determine the resolution of the pion beam.

In order to enhance the flux of negative pions, a position-sensitive single-wire-readout chamber at the second intermediate focus was employed successfully to use a wide momentum bite (about $2.5\times10^{-2}\Delta p/p$) without lowering resolution. For each event the position of the pion in the dispersion plane at $F2$ was measured,

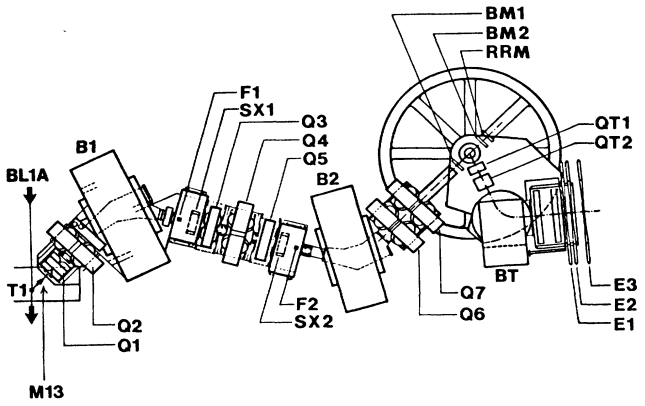

FIG. 1. The $M13$ low-energy pion channel and QQD spectrometer at TRIUMF. $B1$,$B2$ are bending magnets, $Q1$–$Q7$ are quadrupoles, and SX1,SX2 are sextupoles. $F1$ and $F2$ are the chromatic intermediate foci. BT is the QQD dipole and QT1,QT2 are the QQD quadrupoles. $E1$–$E3$ are the rear-end trigger scintillators and BM1,BM2 are the beam-normalization counters. Wire chambers are placed immediately before QT1 and after QT2 and between BT and $E1$. For the π^- measurements, an active slit was placed at $F2$.

which gives its deviation from the central momentum. The energy of the scattered pion was then corrected by this value, effectively compensating for the energy spread of the pion beam. Figure 2 shows a plot of the dispersion at the in-beam wire chamber; Figs. 3(a) and 3(b) show a ^{12}C spectrum before and after the dispersion correction

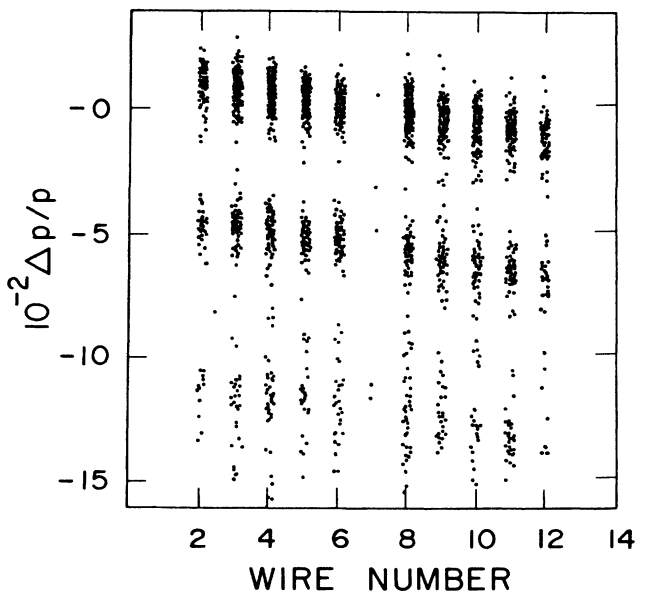

FIG. 2. Dispersion plot at the second chromatic focus in the $M13$ channel. The momentum deviation in percent is plotted with an arbitrary reference point. The three bands correspond to the ground state, the 4.44 MeV, 2^+ state and the 9.64 MeV, 3^- state, respectively. The spacing of the detector wires is 2.54 mm.

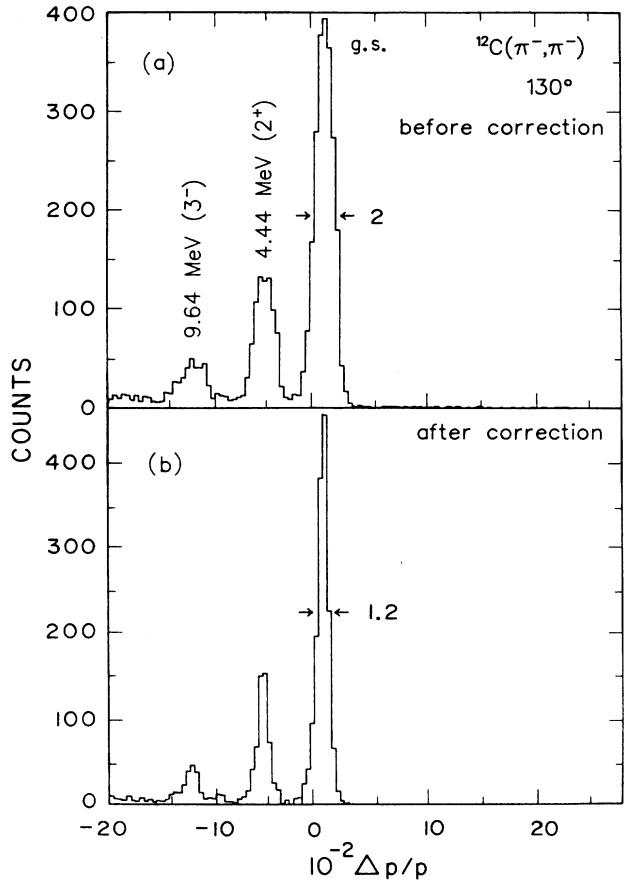

FIG. 3. Spectrum of 50-MeV negative pions scattered from ^{12}C (a) before and (b) after correction for the momentum bite of the channel.

was applied. This technique effectively doubled the flux of negative pions, taking into account the efficiency of the chamber. For positive pions, this chamber could not be operated during the experiment because the absorber present in $F1$ could not stop protons, which resulted in excessive proton counting rate. The channel therefore was set at $1.0\times10^{-2}\Delta p/p$.

The QQD spectrometer consists of two quadrupoles and a dipole and operates in ray-tracing mode. Four multiwire proportional chambers (MWPC's) overdetermine the trajectory of a detected particle in the spectrometer, and the momentum of the particle and its position and angle at the target are calculated from the positions in the MWPC's. Muons from the decay of pions in the spectrometer are discriminated against by checking the trace for consistency. Both the spectrometer and the target chamber were filled with helium to reduce multiple scattering. The combined resolution for channel and spectrometer was about 1.2 MeV FWHM for π^+ and 1 MeV FWHM for π^-. The higher resolution for π^- was due to the momentum correction of the channel.

The event trigger was a coincidence signal among three large plastic scintillators at the rear end of the spectrometer covering the full acceptance and a thin plastic scintillator (0.8 mm) in the beam in front of the target. The in-beam scintillator was also used to determine the fraction of $e^{\pm}$ and $\mu^{\pm}$ contaminations in the beam by measuring the time of flight of the particles passing through the channel.

Cross sections were calculated from the number of counts according to

$$\frac{d\sigma}{d\Omega}=\frac{N}{N_b N_t E_{\mathrm{WC}} f_T f_\pi d_\pi d\Omega}\ , \tag{1}$$

where (typical values are in parentheses) N_b is the number of beam particles, N_t is the number of scatterers per cm^2 in the target, E_{WC} is the wire-chamber efficiency (0.8—0.9), f_T is the fraction of beam hitting the target (0.8—0.9), f_π is the fraction of pions in the beam (0.95), d_π is the fraction of scattered pions that did not decay in the spectrometer (0.7), and $d\Omega$ is the effective solid angle (16 msr). The number of pions emerging from the channel was obtained from the in-beam counter and also from two muon-decay monitors placed at $\pm7°$ relative to the beam.

Systematic uncertainties arise mainly from uncertainties in target thickness and solid angle. The uncertainty in the solid angle is about 10%, while the precision in determining the target thickness might be as poor as 5% (see subsection B below). The uncertainty in beam normalization is negligible compared with these values, so that the total systematic uncertainty is estimated to be less than 12%. This uncertainty, however, cancels in the ratios $d\sigma(\pi^+)/d\sigma(\pi^-)$.

B. Targets

The material for the silicon targets was obtained in the form of silicon powder reduced from SiO_2: natural silicon for the ^{28}Si target (the natural abundance of ^{28}Si is 92.2%) and silicon isotopically enriched to 95.6% for the ^{30}Si target. The natural-silicon powder was chemically pure, while the ^{30}Si contained 13% by weight SiC and 5.5% by weight SiO_2. The material was placed in 2-mm-thick Plexiglas frames and enclosed with 25-μm Kapton windows (50-μm windows in the case of ^{30}Si). The areal density was determined by weighing and measuring the area to be 170 mg/cm^2 for ^{28}Si and 242 mg/cm^2 for ^{30}Si. The precision of this determination is better than 1%, but because some inhomogeneities may exist, an uncertainty no larger than 5% in the areal density is estimated. An empty target of similar dimensions with the windows in place was used to determine the background from the Kapton foils. The empty target was also used to determine precisely the area and position of the active scattering target in the traceback of the spectrometer, since at backward angles, where the projected target area gets smaller, some of the beam hit the Plexiglas frame. All composite targets

were stored in a helium atmosphere a day before mounting in the helium-filled scattering chamber to prevent ballooning of the windows and sagging of the material due to helium diffusing through the Kapton. A CH_2 target that was larger than the beam spot was used to obtain an additional normalization, and also to determine the beam profile at the target location.

III. MEASUREMENTS

Figure 4 shows a spectrum of $^{28}Si(\pi^-,\pi^-)^{28}Si$ at 50 MeV. The ground state and first $J^\pi=2^+$ state at 1.78 MeV clearly stand out. The peak at 6.88 MeV excitation energy arises from the 3^- state at this energy with possible contributions from an unresolved 4^+ state at 6.89 MeV. The absence of counts from normally detectable ^{12}C states indicates that the background from the target windows is negligible. It is evident that the ground state and the 2^+ state are not fully separated, which necessitated the use of a peak fitting procedure to extract their respective cross sections. The peak shape is determined from the ^{12}C normalization spectra. Due to the presence of contaminations in the ^{30}Si target, knowledge of the peak shape was important in determining the area of the peaks. Extensive investigation of the dependence of the extracted area of the peaks on variations in the peak shape enabled us to include the uncertainty associated with the peak-shape parametrization in the statistical uncertainty of the cross sections.

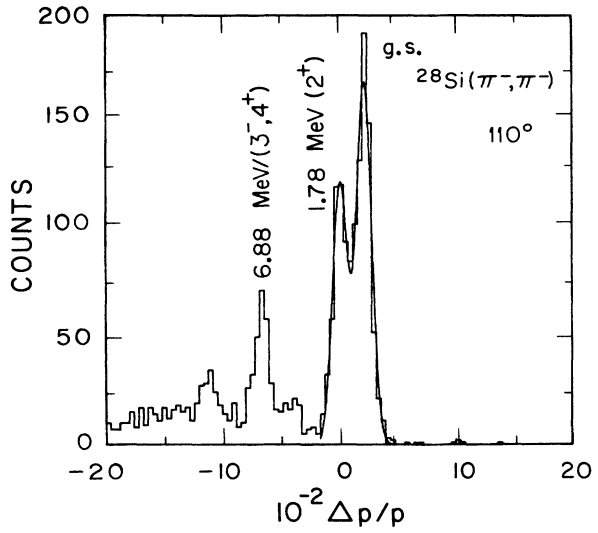

FIG. 4. Spectrum of 50-MeV negative pions scattered from ^{28}Si.

Angular distributions were measured over an angular range from 40° to 128° for ^{28}Si elastic scattering and for the ^{12}C normalization spectra, 40° to 80° for ^{30}Si elastic scattering, and 90° to 128° for ^{28}Si and ^{30}Si inelastic scattering. The cross sections are summarized in Table I. The uncertainties quoted are statistical only and do not include an overall 12% normalization uncertainty. The ^{12}C data are consistent within error bars with the data from

TABLE I. Table of cross sections in the center-of-mass system (uncertainties are statistical only).

θ (deg)	$(d\sigma/d\Omega)(\pi^+)$ (mb/sr)	$(d\sigma/d\Omega)(\pi^-)$ (mb/sr)	$(d\sigma/d\Omega)(\pi^+)$ (mb/sr)	$(d\sigma/d\Omega)(\pi^-)$ (mb/sr)
	^{28}Si, elastic		^{28}Si, 2^+, 1.78 MeV	
38.3	27.1 ±1.7	64.3 ±2.3		
48.3	14.6 ±1.2	25.3 ±1.5		
58.4	9.88±0.82	10.95±0.80		
68.4	9.51±0.54	9.89±0.54		
82.4	13.29±0.67	10.85±0.52		
92.4	9.95±0.28	10.30±0.77	0.73±0.08	1.24±0.13
102.4	9.38±0.43	6.29±0.51	1.60±0.15	1.42±0.17
112.4	6.50±0.34	3.67±0.30	1.63±0.15	2.17±0.18
122.4	4.67±0.34	1.81±0.20	2.49±0.32	2.24±0.33
130.3	3.93±0.24	1.32±0.24	2.59±0.16	2.54±0.33
	^{30}Si, elastic		^{30}Si, 2^+, 2.24 MeV	
38.3	30.1 ±1.6	74.9 ±2.0		
48.3	19.6 ±1.1	30.0 ±1.5		
58.4	11.14±0.72	12.5 ±1.8		
68.4	10.89±0.50	11.5 ±1.1		
78.4	12.90±0.54	14.42±0.86		
92.4			0.667±0.034	1.081±0.095
102.4			0.765±0.066	1.390±0.085
112.4			1.012±0.054	1.49 ±0.13
122.4			1.18 ±0.13	1.5 ±0.092
130.3			1.47 ±0.20	1.58 ±0.15

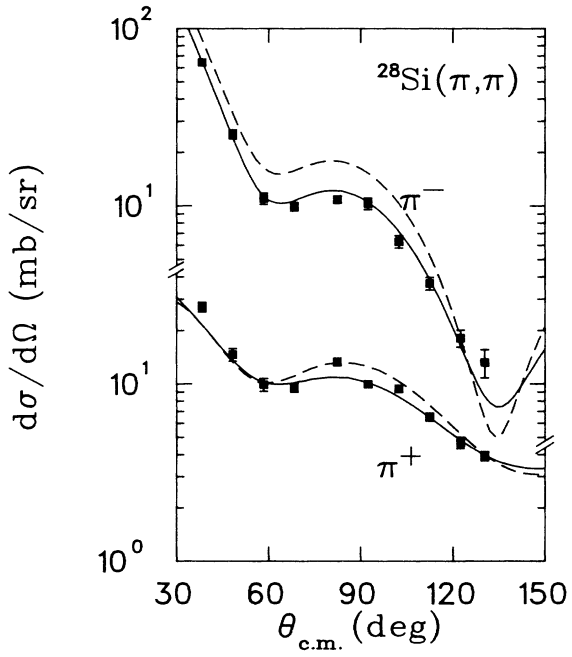

FIG. 5. Angular distributions for elastic scattering of π^+ and π^- from ^{28}Si at 48.9 MeV. The dashed curves represent optical-model calculations using the "set-E" parameters, the solid curves the calculation with our best-fit parameters.

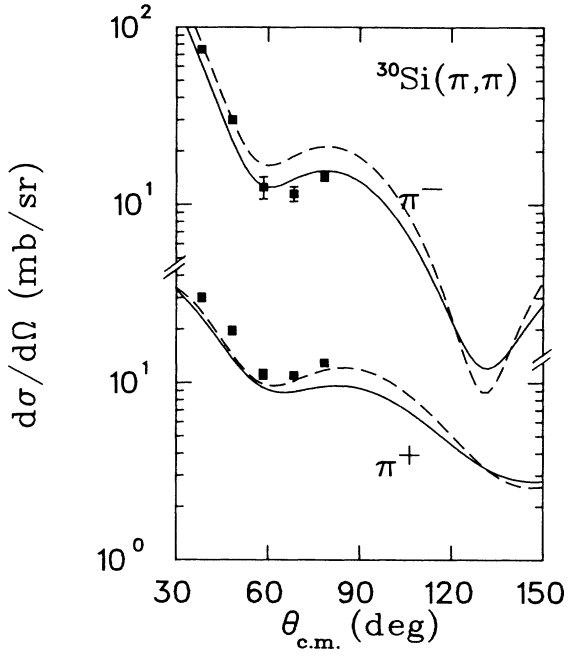

FIG. 7. Angular distributions for elastic scattering of π^+ and π^- from ^{30}Si at 48.7 MeV. The dashed curves represent optical-model calculations using the "set-E" parameters, the solid curves the calculation with the best-fit parameters obtained from the fit to the ^{28}Si data.

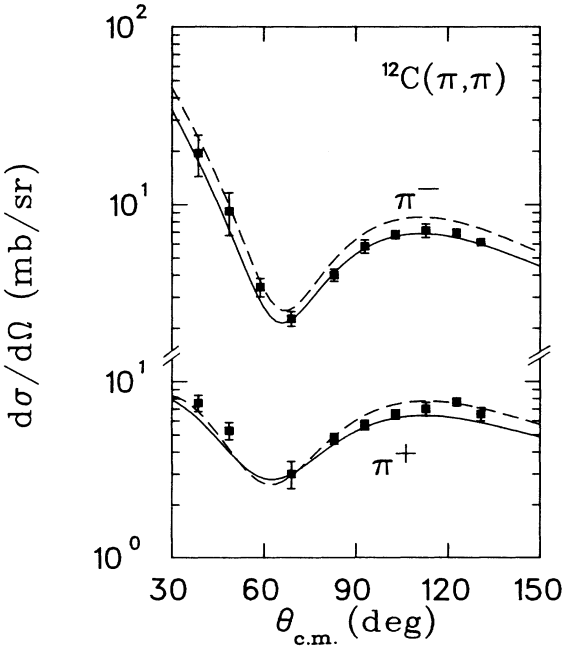

FIG. 6. Angular distributions for elastic scattering of π^+ and π^- from ^{12}C at 48.9 MeV. The solid curves represent optical-model calculations using the best-fit potential obtained from the fit to the ^{28}Si data, the dashed curves the calculation using the "set-E" parameters.

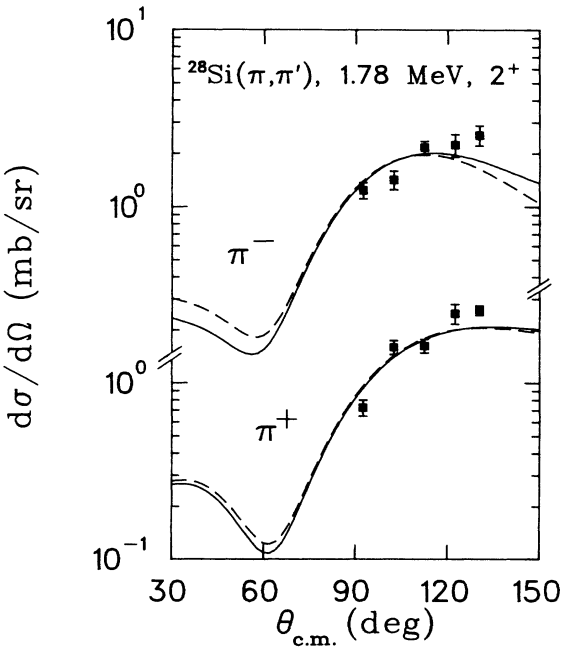

FIG. 8. Angular distributions for inelastic scattering of π^+ and π^- from ^{28}Si at 48.9 MeV. The dashed curves represent the fit using the "set-E" parameters, the solid curves the calculation with the best-fit parameters. The derived ratio of deformation parameters β_n/β_p is 1.10±0.09 for the "set-E" calculation and 1.13±0.09 for the calculation with our best-fit parameters.

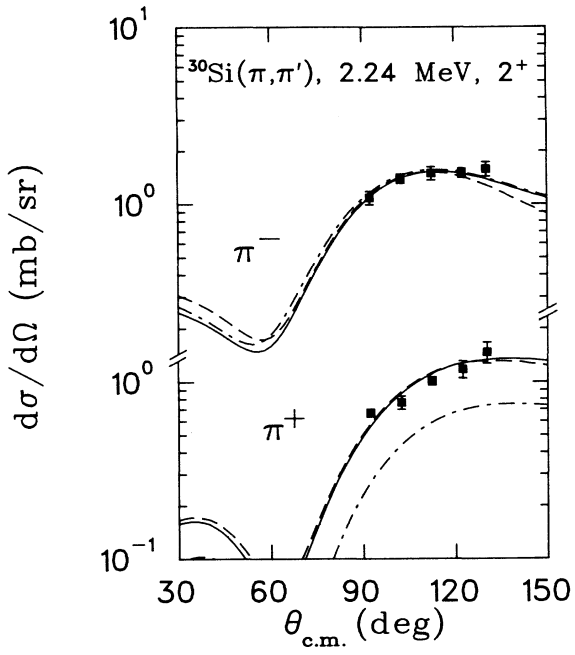

FIG. 9. Angular distributions for inelastic scattering of π^+ and π^- from ^{30}Si 48.7 MeV. The dashed curves represent the fit using the "set-E" parameters, the solid curves the calculation with our best-fit parameters. The derived ratio of deformation parameters β_n/β_p is 0.83±0.08 for the set-E calculation and 0.81±0.08 for the calculation with our best-fit parameters.

Sobie *et al.*[16] and Tacik *et al.*;[4] therefore no renormalization of the cross sections has been done. The previous measurement of elastic π^+ cross sections for ^{28}Si of Dytman *et al.*[17] agrees to within a few percent with our measurement.

The data are shown in Figs. 5–9. Figure 5 shows the elastic cross sections for π^+ and π^- for ^{28}Si, Fig. 6 shows the elastic cross sections for π^+ and π^- for ^{12}C, and Fig. 7 shows the elastic cross sections for π^+ and π^- for ^{30}Si. Figures 8 and 9 show the inelastic cross sections for π^+ and π^- on ^{28}Si and ^{30}Si, respectively.

IV. INTERPRETATION OF RESULTS

A. Elastic scattering

The experimental angular distributions of the elastic cross section have been compared to optical-model calculations using the MSU optical potential.[11–13] It is motivated by the second-order expansion of the multiple-scattering series. The nuclear part of the potential contains terms for s-wave scattering, s-wave absorption, p-wave scattering, p-wave absorption, and the LLEE effect. It has the form (in the notation of Ref. 13)

$$2\omega U = -4\pi \left[p_1(b_0\rho - \epsilon_\pi b_1 \delta\rho) + p_2(B_0\rho^2 - \epsilon_\pi B_1 \rho\,\delta\rho) + \tfrac{1}{2}(1-p_1^{-1})\nabla^2(c_0\rho - \epsilon_\pi c_1 \delta\rho) + \tfrac{1}{2}(1-p_2^{-1})\nabla^2(C_0\rho^2 - \epsilon_\pi C_1 \rho\,\delta\rho) - \nabla \frac{L}{1+(4\pi/3)\lambda L}\nabla \right], \quad (2)$$

where $\rho=\rho(r)$ is the normalized nuclear density, $\delta\rho=\delta\rho(r)$ the neutron-proton density difference, and ϵ_π the pion charge. The p_i are kinematic factors. $L=L(r)$ and λ describe the LLEE effect. The complex parameters $b_{0,1}$ and $c_{0,1}$ describe s- and p-wave single-nucleon scattering. The real parts of $B_{0,1}$ and $C_{0,1}$ describe dispersion effects and nonlinear dynamical effects, and the imaginary parts of $B_{0,1}$ and $C_{0,1}$ describe s- and p-wave true absorption. The subscripts 0 and 1 denote the isoscalar and isovector terms, respectively. In total there are 13 parameters, which are partially constrained by πN phase shifts and pionic-atom data. In the analysis of the MSU group, using the π^+ data available in 1982, several parameter sets were developed, of which their "set E" best described the data at 50 MeV over a wide range of nuclei. The values of the parameters for set E are given in Table II.

The dashed curve in Fig. 5 shows the calculations using the set-E parameters for π^+ and π^- scattering on ^{28}Si. A modified version of the code DWPI (Ref. 18) was used to accommodate the above form of the potential. The π^+ data are reproduced quite well by the set-E calculation, while the description of the π^- data is poor over the full angular range covered by the measurements. This is consistent with the results from other sd-shell nuclei.[4,16] In order to improve the description of the π^- data without destroying the agreement with the π^+ data, we performed

TABLE II. Optical-potential parameters.

	Set E[a]	Our fitted values	
b_0 (fm)	$-0.061+i0.006$	$-0.064+i0.0029$	
b_1 (fm)	$-0.13\ -i0.002$		
c_0 (fm^3)	$0.70\ +i0.028$	$0.621+i0.106$	
c_1 (fm^3)	$0.46\ +i0.013$		
B_0 (fm^4)	$-0.02\ +i0.11$		
C_0 (fm^6)	$0.36\ +i0.54$		
λ	1.4	1.41	
χ^2/ν	48	3.3	
Total reaction cross section for ^{12}C			
			Meas.[b]
π^+ (mb)	114	142	141±9
π^- (mb)	153	182	186±6

[a]From Ref. 13.
[b]From Ref. 23.

a simultaneous fit for π^+ and π^-, varying the scattering parameters b_0 and c_0, and λ. The choice of the particular parameters to be varied was guided in part by observing that in this manner the best of all fits was obtained ($\chi^2=3.3$), although we were able to reproduce the data satisfactorily with several different parameter sets.

The calculation using our fitted parameters is able to reproduce the ^{28}Si data and the ^{12}C data for both π^+ and π^- about equally well. The agreement of the calculation for ^{12}C using our fitted parameters is about as good as for the set-E parameters (Fig. 6). This was also found to be the case for other potential sets tried. We found, however, that the prediction for the total reaction cross section varied for different parameter sets. The reaction cross section has recently been measured to be 141 ± 9 mb for π^+ and 186 ± 6 mb for π^- on ^{12}C at 50 MeV.[19] These values are not reproduced by the set-E calculation, and also are not reproduced when fitting a parameter set following the prescription in Ref. 13 and varying Re b_0 and Re c_0; the reactive parameters must be varied in the fit in order to get agreement with the measured cross sections. The value of 0.106 fm^3 found for the imaginary part of c_0 is somewhat higher than the π-p phase-shift value. It is not grossly inconsistent, however, and, in fact, is consistent with the value of 0.091 fm^3 used by Brown *et al.* in their parameter set "*I*."[20,21] A measurement of the reaction cross section of 50-MeV pions on ^{28}Si would provide important data for determining the potential and also would be useful for model-independent optical-potential calculations, as was pointed out by Friedman.[22] The best-fit potential parameters are also given in Table II; the results of the calculation using the best-fit parameters are shown in Fig. 5 as solid curves.

It has been argued by Sobie *et al.*[16] that π^+ and π^- scattering should be described by different potentials since several approximations are made in the derivation of the form of the potential. However, the energy dependence of the potential parameter was investigated by the MSU group, and their results do not indicate a strong variation, even over a considerable energy range. Other approximations, such as omitting $V_c V_n$ terms in the calculation, have been found to produce negligible effects for several nuclei.[4,16] We certainly have constrained the potential more tightly by fitting the π^+ and π^- cross sections simultaneously.

Figure 7 shows the angular distribution of the elastic-scattering cross section for π^+ and π^- from ^{30}Si. Some discrepancy between the data and the results of our new potential (the solid curves in Fig. 7) does exist, most notably for the π^+ cross section. However, this discrepancy is no worse than that between the data and the set-E results for the π^- cross section.

The π^- cross sections of ^{28}Si and ^{30}Si are used to extract the neutron radius difference between these nuclei, and thus, to determine the neutron radius of ^{30}Si, which has not been measured before. The method has been described in detail in the literature.[23,24] A three-parameter Fermi parametrization for the ground-state density distribution was used throughout the calculations. It has the form

$$\rho(r)=\rho_0\frac{1+w(r/c)^2}{1+\exp[(r-c)/t]}\ , \tag{3}$$

where c is the half-density radius, t is the skin thickness, and w is the "wine-bottle" parameter. The angular distribution for elastic scattering of π^- from ^{28}Si with known ground-state charge-density distribution[25] is reproduced with an optical potential, and the angular distribution for π^- from ^{30}Si was fitted, starting from the ^{28}Si values, and varying the size parameter c for the neutron distribution. The difference in rms neutron radii was found to be 0.023 ± 0.025 fm. The sensitivity to the parameter set used is small at forward angles. (The same method cannot be applied to the π^+ data, since the ground-state densities are known). Because the data base is too limited, we also could not fit the isovector parameters in the potential in a meaningful way to reduce the discrepancy for the π^+ data; therefore, we kept them fixed at the set-E values. The ground-state-density-distribution parameters used are given in Table III. The values for the proton distributions are taken from recent electron-scattering experiments;[25] and for the $N=Z$ nucleus ^{28}Si, r_n is assumed to be equal to r_p.

B. Inelastic scattering

The proton and neutron transition densities for the first 2^+ excited state has been has been parametrized with the Tassie model[26] as

$$\rho_{tr}(r)=\beta_2 r\frac{d\rho}{dr}\ , \tag{4}$$

where ρ is the ground-state matter-density distribution. The proportionality factor β_2 can be related to the quadrupole part of the nuclear deformation and thus can be compared to the transition probability since

TABLE III. Parameters of the ground-state density distributions.

Nucleus	c (fm)	t (fm)	w	$\langle r^2\rangle^{1/2}$ (fm)
^{28}Si[a] n,p	3.188±0.009	2.549±0.012	−0.233±0.009	2.963±0.006
^{30}Si[a] p	3.060±0.021	2.429±0.010	−0.078±0.022	3.057±0.011
^{30}Si[b] n	3.218±0.025	2.549±0.012	−0.233±0.009	2.986±0.025

[a]From Ref. 25.
[b]Present work.

$$B(E2, 0^+ \rightarrow 2^+) = |M_p|^2 = \left[\frac{3Z}{4\pi} R_0^2\right]^2 \beta_2^2 , \quad (5)$$

where $B(E2, 0^+ \rightarrow 2^+)$ is the transition probability, M_p the transition-matrix element, and R_0 the effective nuclear radius.[27] Assuming isospin conservation, one has $M_n(N,Z) = M_p(Z,N)$, i.e.,

$$|M_n|^2 = \left[\frac{3N}{4\pi} R_0^2\right]^2 \beta_2^2 . \quad (6)$$

This relation is not necessarily exact, however, since Coulomb effects will cause deviations from this rule. For the $A = 30$ isospin triplet, the lifetimes of the first $J^\pi = 2^+$ states have been measured recently by Doppler-shift attenuation measurements;[28] the $B(E2)$ values are calculated from these via

$$B(E2, 0^+ \rightarrow 2^+) = 4.078 \times 10^{-9}/(\tau E^5) , \quad (7)$$

where E is the transition energy in MeV and τ is the lifetime of the excited state in sec, taking into account possible decay via competing branches.

Our inelastic-scattering data have been analyzed with DWIA calculations using the optical potential given by Eq. (2) with both the set-E parameters and the parameter set found to describe best the π^+ and π^- elastic-scattering data. The shape of the angular distribution is given by the angular-momentum transfer $\Delta l = 2$ of the reaction, while the β parameters determine the magnitude of the cross sections. The ground-state density parameters that we use are the ones in Table III. Since the inelastic cross section is proportional to $\beta^2 r$, uncertainties in the radii have a relatively minor effect on the precision of the extracted value for β. Figure 8 shows the inelastic-scattering data together with the calculated cross sections for ^{28}Si; the β parameters for protons and neutrons were varied simultaneously to fit the data. The extracted ratio $\beta_n/\beta_p = M_n/M_p$ is 1.10 ± 0.09 using the set-E parameters and 1.13 ± 0.09 using our best-fit parameters. Both values are consistent (although just barely) with the theoretical ratio of unity. The particular choice of optical parameters does not significantly affect the ratio β_n/β_p, but the absolute values do show a certain parameter dependence. The absolute values obtained using our best-fit parameter set are $\beta_n = 0.42 \pm 0.04$ and $\beta_p = 0.47 \pm 0.04$, close to the electromagnetic value, which lies between 0.40 (Ref. 29) and 0.42 (Ref. 30).

The angular distributions for ^{30}Si are shown in Fig. 9 together with the results of the calculations. We extract a ratio β_n/β_p of 0.83 ± 0.08 and 0.81 ± 0.08 for the set-E and the best-fit potential, respectively; the corresponding absolute values are $\beta_n = 0.327 \pm 0.040$ and $\beta_p = 0.407 \pm 0.043$, using our best-fit parameters. Our value for the ratio clearly disagrees with the ratio of 1.06 ± 0.05 derived from the lifetime data of Alexander.[28] The dash-dotted line in Fig. 9 represents the calculation using the values from the lifetime measurements for the β parameters ($\beta_n = 0.33$, $\beta_p = 0.31$), illustrating the magnitude of this discrepancy as well as the sensitivity of the low-energy pion-scattering technique. The discrepancy suggests that it might not be correct to compare directly the matrix-element ratios derived from pion scattering with those obtained from mirror nuclei.

TABLE IV. Transition-matrix-element ratios for *sd*-shell nuclei.

Nucleus	M_n/M_p (mirror nucleus)	M_n/M_p (low-energy pionic)	Ratio
^{18}O	2.07 ± 0.22 [a]	1.81 ± 0.15 [b]	1.14 ± 0.15
^{26}Mg	1.05 ± 0.07 [c]	0.83 ± 0.06 [d]	1.27 ± 0.12
^{30}Si	1.22 ± 0.06 [e]	0.93 ± 0.09 [f]	1.32 ± 0.14
^{34}S	1.39 ± 0.19 [g]	1.14 ± 0.08 [h]	1.22 ± 0.18

[a] From Ref. 31.
[b] From Ref. 4.
[c] From Ref. 34.
[d] From Ref. 4.
[e] From Ref. 28.
[f] Present work.
[g] From Ref. 35.
[h] From Ref. 16.

At this point, it is instructive to examine the values of M_n/M_p for other nuclei for which transition data to 2^+ states are available. Table IV compares the ratios of transition-matrix elements M_n/M_p obtained by low-energy pion scattering for ^{18}O, ^{26}Mg, ^{30}Si, and ^{34}S with the values obtained by the mirror-nucleus method. The electromagnetic ratio is always higher, by factors ranging from 1.14 to 1.32. For ^{18}O, a Coulomb-correction factor of 1.1 was derived in Ref. 31. This factor, which was considered extreme by Bernstein *et al.* in a later publication,[7] is included in the quoted ratio, and reduces the discrepancy but does not eliminate it.

Recently, Kelly *et al.*[12] compared data for the scattering of 135-MeV protons from ^{18}O with electron-scattering data and derived for M_n/M_p a value of 2.06 ± 0.03, in close agreement with the mirror-nucleus value. The values of M_n/M_p obtained from scattering of *resonance*-energy pions on ^{18}O and ^{26}Mg are about 1.6 (Refs. 1, 2, and 33) and 0.62 ± 0.14 (Ref. 3), in agreement with the low-energy pionic values. The uncertainty as to how to describe the pion-nucleus interaction at low energies might account for some of the discrepancies observed. However, since the π-N interaction at resonance energies is believed to be well understood, the agreement of the low- and high-energy ratios supports the validity of the interpretation of the low-energy pion data.

V. SUMMARY AND CONCLUSIONS

In the present work the angular distributions of the differential cross sections for scattering of 50-MeV π^+ and π^- from ^{28}Si and ^{30}Si have been measured. The elastic cross sections enlarge the existing data base for pion-nucleus scattering, which is needed to constrain the optical potential used to describe low-energy pion scattering. The inelastic-scattering data are used to determine the ratio of neutron and proton transition matrix elements M_n/M_p, which is compared with the same ratio obtained with other probes.

The results from the present experiment are consistent with other pion-scattering data. The elastic π^+ cross section is reasonably well described by a second-order

optical-potential calculation using the global set-E parameters.[13] However, the calculated π^- cross section disagrees with the data. This disagreement could have been anticipated from the results of previous measurements on other *sd*-shell nuclei, and may very well be due to the fact that no π^- scattering data were available at the time the global fit was performed. It is, however, possible to find a potential that simultaneously describes both elastic π^+ and elastic π^- data for ^{28}Si and also for ^{12}C, by adjusting the single-nucleon scattering parameters. The potential found in this manner also gives the correct total reaction cross section for 50-MeV $\pi^\pm$ on ^{12}C, in contrast with the results of the set-E calculation.

The inelastic cross section for the transition to the first 2^+ excited state gives the ratio of proton and neutron transition matrix elements for ^{28}Si (1.13 ± 0.09) and ^{30}Si (0.93 ± 0.09). These results are consistent with pion-scattering results for other nuclei in the sense that the values for $N=Z+2$ nuclei are consistently smaller than the values obtained by the mirror-nucleus method. However, our ratio for ^{30}Si shows the most significant deviation from any mirror-nucleus value measured to date. Coulomb corrections might account for part of this deviation, but the theoretical situation is not clear. The value for M_n/M_p or 1.13 ± 0.09 for ^{28}Si is nearly consistent with unity. Interestingly, Sobie *et al.* found this ratio for ^{32}S to be 1.12 ± 0.07 when using the same potential for π^+ and π^-.[16] The isovector sensitivity of low-energy pions appears now to be established and the derived ratios of transition matrix elements generally follow the trend of the ratios derived from mirror nuclei. Our study of ^{30}Si shows quantitative differences that indicate the need for further study of both the pion-nucleus interaction and the Coulomb corrections used in electromagnetic measurements.

ACKNOWLEDGMENTS

The authors gratefully acknowledge the support of the TRIUMF staff. The ^{30}Si sample was supplied by the Lawrence Livermore Laboratory. This work was supported by the Natural Sciences and Engineering Research Council of Canada and by the U.S. Department of Energy under Contract No. W7405-ENG-48 and DE-FG05-86ER40285, respectively. The work of U.W. was supported in part by the Deutscher Akademischer Austauschdienst.

*Present address: TRIUMF, 4004 Wesbrook Mall, Vancouver, British Columbia, Canada V6T 2A3.

†Present address: Brookhaven National Laboratory, Upton, NY 11973.

‡Present address: Physikalisches Institut der Universität Tübingen, D-7400 Tübingen, Federal Republic of Germany.

§Present address: Universität Basel, CH-4056 Basel, Switzerland.

**Present address: Israel Air Industries, Tel Aviv, Israel.

††Present address: Department of Physics, Kent State University, Kent, OH 42422.

[1]S. Iversen, A Obst, K. K. Seth, H. A. Thiessen, C. L. Morris, N. Tanaka, E. Smith, J. F. Amann, R. L. Boudrie, G. Burleson, M. Devereux, L. W. Swenson, P. Varghese, K. Boyer, W. J. Brathwaite, W. Cottingame, and C. F. Moore, Phys. Rev. Lett. **40**, 17 (1978).

[2]C. Lunke, R. Corfu, J. P. Egger, P. Gretillat, J. Piffaretti, E. Schwarz, J. Jansen, C. Perrin, and B. M. Preedom, Phys. Lett. **78B**, 201 (1978).

[3]C. A. Wiedner, J. A. Nolen, Jr., W. Saathoff, R. E. Tribble, J. Bolger, J. Zichy, K. Stricker, H. McManus, and J. A. Carr, Phys. Lett. **78B**, 26 (1978).

[4]R. Tacik, Ph.D. thesis, University of British Columbia, 1984 (unpublished); R. Tacik, K. L. Erdman, R. R. Johnson, H. W. Roser, D. R. Gill, E. W. Blackmore, R. J. Sobie, T. E. Drake, S. Martin, and C. A. Wiedner, Phys. Rev. Lett. **52**, 1276 (1984).

[5]V. A. Madsen, V. R. Brown, and J. D. Anderson, Phys. Rev. C **12**, 1205 (1975).

[6]A. M. Bernstein, V. R. Brown, and V. A. Madsen, Phys. Lett. **71B**, 48 (1977).

[7]A. M. Bernstein, V. R. Brown, and V. A. Madsen, Phys. Rev. Lett. **42**, 425 (1979).

[8]A. M. Bernstein, V. R. Brown, and V. A. Madsen, Phys. Lett. **103B**, 255 (1981).

[9]A. M. Bernstein, V. R. Brown, and V. A. Madsen, Commun. Nucl. Part. Phys. **11**, 203 (1983).

[10]L. S. Kisslinger, Phys. Rev. **98**, 761 (1955).

[11]K. Stricker, H. McManus, and J. A. Carr, Phys. Rev. C **19**, 929 (1979).

[12]K. Stricker, J. A. Carr, and H. McManus, Phys. Rev. C **22**, 2043 (1980).

[13]J. A. Carr, H. McManus, and K. Stricker-Bauer, Phys. Rev. C **25**, 952 (1982).

[14]C. J. Oram, J. B. Warren, G. M. Marshall, and J. Doornbos, Nucl. Instrum. Methods **179**, 95 (1981).

[15]R. J. Sobie, T. E. Drake, B. M. Barnett, K. L. Erdman, W. Gyles, R. R. Johnson, H. W. Roser, R. Tacik, E. W. Blackmore, D. R. Gill, S. Martin, C. A. Wiedner, and T. Masterson, Nucl. Instrum. Methods **219**, 501 (1984).

[16]R. J. Sobie, Ph.D. thesis, University of Toronto, 1984 (unpublished); R. J. Sobie, T. E. Drake, K. L. Erdman, R. R. Johnson, H. W. Roser, R. Tacik, E. W. Blackmore, D. R. Gill, S. Martin, C. A. Wiedner, and T. Masterson, Phys. Rev. C **30**, 1612 (1984).

[17]S. A. Dytman, J. F. Amann, P. D. Barnes, J. N. Craig, K. G. R. Doss, R. A. Eisenstein, J. D. Sherman, W. R. Wharton, G. R. Burleson, S. L. Verbeck, R. J. Peterson, and H. A. Thiessen, Phys. Rev. C **19**, 971 (1979).

[18]R. A. Eisenstein and G. A. Miller, Comput. Phys. Commun. **11**, 95 (1976).

[19]R. R. Johnson and E. Friedman, private communication.

[20]G. E. Brown, B. K. Jennings, and V. I. Rostokin, Phys. Rep. **50**, 227 (1979).

[21]B. K. Jennings, private communications.

[22]E. Friedman, Phys. Rev. C **28**, 1264 (1983).

[23]R. R. Johnson, T. Masterson, B. Bassalleck, W. Gyles, T. Marks, K. L. Erdman, A. W. Thomas, D. R. Gill, E. Rost, J. J. Karaushaar, J. Alster, C. Sabev, J. Arvieux, and M. Krell, Phys. Rev. Lett. **43**, 844 (1979).

[24]W. Gyles, Ph.D. thesis, University of British Columbia, 1984 (unpublished); W. Gyles, B. M. Barnett, R. Tacik, K. L. Erdman, R. R. Johnson, G. J. Lolos, H. W. Roser, K. A. Aniol, F. Entezami, E. L. Mathie, D. R. Gill, E. W. Blackmore, C. A. Wiedner, S. Martin, R. J. Sobie, and T. E. Drake, Nucl. Phys. **A439**, 598 (1985).

[25]H. Miessen, Ph.D. thesis, Johannes Gutenberg Universität Mainz, 1982 (unpublished); H. Rothhaas, H. Miessen, and B. L. Berman, to be published.

[26]L. J. Tassie, Aust. J. Phys. **9**, 407 (1956).

[27]A. Bohr and B. R. Mottelson, *Nuclear Structure* (Benjamin, Reading, Mass., 1975), Vol. II.

[28]T. K. Alexander, G. C. Ball, J. S. Forster, W. G. Davies, I. V. Mitchell, and H. B. Mak, Phys. Rev. Lett. **49**, 438 (1982).

[29]P. H. Stelson and L. Grodzins, Nucl. Data **A1**, 21 (1965).

[30]J. S. Forster, T. K. Alexander, G. C. Ball, W. G. Davies, I. V. Mitchell, and K. B. Winterbon, Nucl. Phys. **A313**, 397 (1979).

[31]B. A. Brown, A. Arima, and J. B. McGrory, Nucl. Phys. **A277**, 77 (1977).

[32]J. Kelly, W. Bertozzi, T. N. Buti, J. M. Finn, F. W. Hersman, M. V. Hynes, C. Hyde-Wright, B. E. Norum, A. D. Bacher, G. T. Emery, C. C. Foster, W. P. Jones, D. W. Miller, B. L. Berman, J. A. Carr, and F. Petrovich, Phys. Lett. **169B**, 157 (1986).

[33]T. K. Alexander, G. C. Ball, W. G. Davies, J. S. Forster, and I. V. Mitchell, Phys. Lett. **113B**, 132 (1982).

[34]S. Iversen, H. Nann, A. Obst, K. K. Seth, N. Tanaka, C. L. Morris, H. A. Thiessen, K. Boyer, W. Cottingame, C. F. Moore, R. L. Boudrie, and D. Dehnhard, Phys. Lett. **82B**, 51 (1979).

[35]P. M. Endt and C. Van der Leun, Nucl. Phys. **A310**, 1 (1978).